Strain-induced variations of electronic energy band edges of embedded semiconductor quantum dots in half-space substrates

Ernie Pan,[1,a)] Yu Zou,[1] Peter W. Chung,[2] and John D. Albrecht[3]
[1]*Computer Modeling and Simulation Group, College of Engineering, University of Akron, Akron, Ohio 44325, USA*
[2]*U.S. Army Research Laboratory, Aberdeen Proving Ground, Maryland 21005, USA*
[3]*Air Force Research Laboratory, WPAFB, Ohio 45433, USA*

(Received 15 July 2009; accepted 24 August 2009; published online 7 October 2009)

The strain-induced local electronic band edge states in semiconductor quantum dots (QDs) are studied using a $\mathbf{k}\cdot\mathbf{p}$ description of the electronic eigenstates coupled with the induced lattice strain as calculated using the continuum mechanics (CM) description. In the CM method, the misfit-lattice induced strain can be reduced to an analytical expression that is straightforward to evaluate numerically. Different from most previous analyses for QDs in infinite spaces, we address cubic and pyramidal QDs located in half-space substrates with different lattice orientations, which more realistically describe experimental situations in most instances. The band edges within the cubic and pyramidal InAs QDs embedded in GaAs substrates are predicted within the six-band $\mathbf{k}\cdot\mathbf{p}$ basis via both a published approximation and the presented exact approach. Comparison of the strain-induced local band edge shows that the approximate method adopted previously in literature could result in a substantial error near the interface region of the QD. The strain-induced band edges along the bottom center line of the QD can differ by a factor of 2 between the two approaches. Furthermore, the effect of the free surface on the strain-induced band edges is studied by varying the depth of the buried QD. When the QD is moved away from the surface, the band edges converge in a consistent way to the infinite-space solution. Comparison with available experimental results validates our exact model within the half-space substrate and shows the importance of treating the surface in a theoretically rigorous way. © *2009 American Institute of Physics*. [doi:10.1063/1.3234383]

I. INTRODUCTION

Quantum-dot (QD) heterostructures have been increasingly sought for applications as novel materials and devices such as gain media for semiconductor lasers. Their unique properties arise from quantum confinement and are known to be further sensitive to strain-perturbed fields that modify the electronic states, and subsequently the optoelectronic properties.[1–3] Strain is increasingly a useful variable with which bandgap energies, and subsequently exciton energies, can be designed into devices.[4] The sensitivity of the bands to strains can be substantial. The strain-induced level shifts in the bandgap of InAs/GaAs QDs in some cases may approach the gap sizes of the semiconductor.[5]

There are a couple of theoretical/numerical studies on the effect of strain on the band edges in pyramidal QDs. For example, an original technique based on a plane-wave expansion method to calculate the electron and hole wave spectra was presented by Andreev and O'Reilly,[6] including the three-dimensional strain and built-in electric field distributions. Ranjan *et al.*[7] studied the optical properties of strained GaN QDs using a tight-binding method. Grundmann *et al.*[8] simulated numerically a pyramidal QD on a thin wetting layer using the finite difference method and also calculated the corresponding electronic structure and the optical-phonon energies. The strain distribution of self-assembled pyramidal InGaAs/GaAs QDs and the dependence of the biaxial and hydrostatic components on the QD volume, aspect ratio, and composition were calculated by Califano and Harrison[9] using Green's function-based technique. With refined meshes and grids, these numerical methods can predict very good strain profiles and confining potentials.

In general, the theories/models for analyzing the misfit-lattice induced strain field and the corresponding band structure in low-dimensional QD systems can be categorized as the continuum mechanics (CM) based method[10–13] and the valence force field[14,15] method for the calculation of the strain field, and the empirical tight-binding model,[16–18] empirical pseudopotential model,[19,20] and the $\mathbf{k}\cdot\mathbf{p}$ model[21] for the calculation of the band structure. However, we point out that in most of the previous research, the QD was assumed to be in an infinite-space material matrix or substrate. Furthermore, in applying the six-band $\mathbf{k}\cdot\mathbf{p}$ model for bandgap edge calculation, the induced shear strain and the normal strain difference were both neglected.

In this paper, we assume that the QD is buried within a half-space substrate where the distance from the QD to the surface is arbitrary. As such, the induced strain field and the local band edge will be influenced by the existence of a free boundary, resulting in different strain and band edge features as compared to those in an infinite space. Further, to calculate the elastic field induced by the QD, the analytical Green's function method presented by Pan *et al.*[22] is employed, where the QD surface is approximated by a number of flat triangles so that the required boundary integration can be carried out exactly. Based on our analytical solution for the induced strain field, we predict the strain-related local band edge for the InAs QD within the GaAs substrate using

a)Electronic mail: pan2@uakron.edu.

the six-band $\mathbf{k}\cdot\mathbf{p}$ model (for both the exact and approximate approaches). Our numerical results show that the free surface of the substrate could have a significant influence on the bandgap edge and that the exact $\mathbf{k}\cdot\mathbf{p}$ model has to be employed in the strain-induced bandgap prediction. This conclusion is further confirmed by previous experimental results against which the approximate six-band $\mathbf{k}\cdot\mathbf{p}$ model shows a large error in the band edge calculation.

This paper is organized as follows: Green's function method for calculating the misfit-lattice induced elastic strain and the analytical multiband $\mathbf{k}\cdot\mathbf{p}$ model for evaluating the strain-induced band edge shifts are introduced in Sec. II. Numerical results for cubic and pyramidal InAs QDs within GaAs (001) and (111) substrates are presented in Sec. III, along with a comparison to published experimental data for validation. Conclusions are drawn in Sec. IV.

II. MISFIT-LATTICE INDUCED ELASTIC STRAIN FIELD AND K·P MODEL FOR ZINCBLENDE QD

To simplify the strain calculation, we adopt the Eshelby inclusion approach, which assumes that the material properties between the QD and the substrate are the same.[6,23] By doing so, the induced elastic strain can be obtained by simple integration of the analytic Green's functions over the QD surface.[22] Furthermore, for the QD made of piecewise flat surfaces, the involved surface integration can be exactly carried out. Therefore, the QD-induced elastic strain can be accurately predicted based on our Green's function method.[22,24–27] We point out that although the complex inhomogeneity model was proposed to study the strained quantum structure,[28] finding reliable material properties in the QD and quantum wire is still a challenge.[29]

In order to calculate the band edges, we use the established multiband $\mathbf{k}\cdot\mathbf{p}$ method that accounts for the strain effects with related parameters being determined empirically and/or experimentally.[30] Without sacrificing the salient physical characteristics for this investigation, the Hamiltonian matrix could be further simplified by suppressing the shear strain and the strain difference between γ_{xx} and γ_{yy}.[15,31,32] By doing so, one is able to derive simple closed-form expressions for the electronic states at the conduction band (CB) and valence band (VB) edges and evaluate the relative significance of different treatments of the lattice strain. It is apparent that this approximation would be acceptable if the shear strain is very small and the deformation is such that $\gamma_{xx}=\gamma_{yy}$. In general, however, one should be cautious in making such an assumption, as will be illustrated later with numerical examples.

We limit our consideration to the local band edges (at $\mathbf{k}=0$) pertinent to many of the direct bandgap semiconductor QD systems of this class. At the zone center the CB and VB models can be decoupled and the latter can be further characterized by a six-band Hamiltonian. We adopt the accepted standard notation for wave function basis functions as follows:[33]

$$
\begin{aligned}
\left|\tfrac{3}{2},\tfrac{3}{2}\right\rangle &= -\tfrac{1}{\sqrt{2}}|(x+iy)\uparrow\rangle,\\
\left|\tfrac{3}{2},\tfrac{1}{2}\right\rangle &= \tfrac{1}{\sqrt{6}}|-(x+iy)\downarrow+2z\uparrow\rangle,\\
\left|\tfrac{3}{2},-\tfrac{1}{2}\right\rangle &= \tfrac{1}{\sqrt{6}}|(x-iy)\uparrow+2z\downarrow\rangle,\\
\left|\tfrac{3}{2},-\tfrac{3}{2}\right\rangle &= \tfrac{1}{\sqrt{2}}|(x-iy)\downarrow\rangle,\\
\left|\tfrac{1}{2},\tfrac{1}{2}\right\rangle &= \tfrac{1}{\sqrt{3}}|(x+iy)\downarrow+z\uparrow\rangle,\\
\left|\tfrac{1}{2},-\tfrac{1}{2}\right\rangle &= \tfrac{1}{\sqrt{3}}|(x-iy)\uparrow-z\downarrow\rangle,
\end{aligned}
\tag{1}
$$

where $|x\rangle$, $|y\rangle$, and $|z\rangle$ indicate the symmetry of the VB zone center states, and $\downarrow$ and $\uparrow$ denote the spin orientations. According to the theory of Luttinger and Kohn,[34] and Bir and Pikus,[35] the VB band structure (at $\mathbf{k}=0$) of a strained bulk semiconductor can be described by the following 6×6 Hamiltonian in the envelope-function space [including the heavy hole (HH) ($|3/2,\ \pm3/2\rangle$), light hole (LH) ($|3/2,\ \pm1/2\rangle$), and spin-orbit split-off bands (SO) ($|1/2,\ \pm1/2\rangle$)]:

$$
H=-\begin{pmatrix}
P_\gamma+Q_\gamma & -S_\gamma & R_\gamma & 0 & -\frac{1}{\sqrt{2}}S_\gamma & \sqrt{2}R_\gamma \\
-S_\gamma^{+} & P_\gamma-Q_\gamma & 0 & R_\gamma & -\sqrt{2}Q_\gamma & \sqrt{\frac{3}{2}}S_\gamma \\
R_\gamma^{+} & 0 & P_\gamma-Q_\gamma & S_\gamma & \sqrt{\frac{3}{2}}S_\gamma^{+} & \sqrt{2}Q_\gamma \\
0 & R_\gamma^{+} & S_\gamma^{+} & P_\gamma+Q_\gamma & -\sqrt{2}R_\gamma^{+} & -\frac{1}{\sqrt{2}}S_\gamma^{+} \\
-\frac{1}{\sqrt{2}}S_\gamma^{+} & -\sqrt{2}Q_\gamma & \sqrt{\frac{3}{2}}S_\gamma & -\sqrt{2}R_\gamma & P_\gamma+\Delta & 0 \\
\sqrt{2}R_\gamma^{+} & \sqrt{\frac{3}{2}}S_\gamma^{+} & \sqrt{2}Q_\gamma & -\frac{1}{\sqrt{2}}S_\gamma & 0 & P_\gamma+\Delta
\end{pmatrix}
\begin{matrix}
\left|\frac{3}{2},\frac{3}{2}\right\rangle \\
\left|\frac{3}{2},\frac{1}{2}\right\rangle \\
\left|\frac{3}{2},-\frac{1}{2}\right\rangle \\
\left|\frac{3}{2},-\frac{3}{2}\right\rangle \\
\left|\frac{1}{2},\frac{1}{2}\right\rangle \\
\left|\frac{1}{2},-\frac{1}{2}\right\rangle
\end{matrix},
\tag{2}
$$

where Δ is the spin-orbit split-off energy and "+" denotes the Hermitian conjugate of the matrix elements. The key strain-dependent elements in the matrix are defined as

$$P_\gamma = -a_v \gamma_H, \tag{3a}$$

$$Q_\gamma = -\frac{b}{2}\gamma_B, \tag{3b}$$

$$R_\gamma = \frac{\sqrt{3}}{2} b(\gamma_{xx} - \gamma_{yy}) - id\gamma_{xy}, \tag{3c}$$

$$S_\gamma = -d(\gamma_{xz} - i\gamma_{yz}), \tag{3d}$$

where a_c, a_v, b, and d are the Pikus-Bir deformation potential constants for the CB and VB; and $\gamma_H = \gamma_{xx} + \gamma_{yy} + \gamma_{zz}$ and $\gamma_B = \gamma_{xx} + \gamma_{yy} - 2\gamma_{zz}$ are defined as the hydrostatic and biaxial strains, respectively.

We will focus our attention on the local band edge modification based on the induced strain, as in Pryor's paper.[36] That is, we will calculate the eigenvalues of strain-dependent Hamiltonian (2). In general, the eigenvalues of Eq. (2) need to be solved numerically. However, if one further assumes that $S_\gamma = R_\gamma = 0$, i.e., ignoring the shear strain and the normal strain difference between γ_{xx} and γ_{yy}, then the eigenvalues of matrix (2), as the strain-induced band edge shifts of VB, can be obtained analytically as

$$E_{\mathrm{HH}} = -P_\gamma - Q_\gamma = a_v \gamma_H + \frac{b}{2}\gamma_B, \tag{4a}$$

$$E_{\mathrm{LH}} = -P_\gamma + \frac{1}{2}(Q_\gamma - \Delta + \sqrt{\Delta^2 + 2\Delta Q_\gamma + 9Q_\gamma^2}) = a_v \gamma_H - \frac{b}{4}\gamma_B - \frac{1}{2}\Delta + \frac{1}{2}\sqrt{\Delta^2 - \Delta b \gamma_B + \frac{9}{4}b^2\gamma_B^2}, \tag{4b}$$

$$E_{\mathrm{SO}} = -P_\gamma + \frac{1}{2}(Q_\gamma - \Delta - \sqrt{\Delta^2 + 2\Delta Q_\gamma + 9Q_\gamma^2}) = a_v \gamma_H - \frac{b}{4}\gamma_B - \frac{1}{2}\Delta - \frac{1}{2}\sqrt{\Delta^2 - \Delta b \gamma_B + \frac{9}{4}b^2\gamma_B^2}. \tag{4c}$$

On the other hand, by assuming the unstrained bandgap as E_{g0}, the relative CB edge energy is given by

$$E_C = E_{g0} + a_c \gamma_H. \tag{5}$$

III. NUMERICAL RESULTS AND COMPARISON TO EXPERIMENTS

In this section, cubic and pyramidal InAs QDs in (001) and (111) GaAs half-space substrates are investigated). The misfit-lattice eigenstrain in the QD is hydrostatic, i.e., $\gamma_{xx}^* = \gamma_{yy}^* = \gamma_{zz}^* = 0.07$. The origin (0,0,0) of the coordinate system is on the surface of the half plane, and the z-axis points down vertically. Both cubic and pyramidal QDs have the same height ($h = 4$ nm), same volume, and the same vertical distance to the surface ($d = 4$ nm) from their middle plane but with different base lengths ($b = 8.62$ nm for cubic and $b = 14.93$ nm for pyramidal QD). Other involved material properties and parameters are listed in the Appendix. Numerical results are presented via both approximate method (4) where the shear strain and the normal strain difference between γ_{xx} and γ_{yy} are neglected and the exact method where the eigenenergies of Hamiltonian (2) are solved directly without the above approximation. The results for the strain-induced CB edge based on Eq. (5) are also shown in the figures. Furthermore, comparison with the available experimental results validates our exact model within the half-space substrate, and thus demonstrates that the influence of the surface is important and that the approximate approach for band edge calculation is not valid near the boundary of the QDs. We point out that in the (111)-direction case, there will be an induced piezoelectric field. However, this induced piezoelectric field has a negligible effect on the bandgap within the QD for group III-V semiconductors since the piezoelectric couplings in these materials are very weak.[37,38] Its influence outside the QD could be important (e.g., lowers the symmetry of the involved system, leads to a lifting of degeneracy, etc).[8] This will be addressed in the future using the fully coupled piezoelectric model, which can be applied to the strongly coupled III nitrides as well as the weakly coupled group III-V semiconductors.[38]

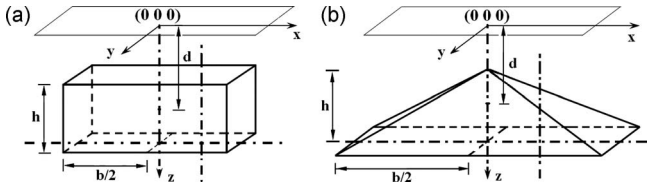

FIG. 1. Schematic of InAs QDs in GaAs substrates: cubic QD in (a) and pyramid QD in (b). Both QDs have the same distance between the body center and the surface of half plane: $d = 4$ nm; strain and band edge results are along the dashed-dotted lines and the z-axis.

A. Local band edges in a cubic InAs QD embedded in (001) and (111) GaAs half-space substrates

The local band edge energies within the embedded InAs QD along three dashed-dotted lines [see Fig. 1(a)] are investigated via both the exact and approximate methods. The first line is on the bottom plane of the cubic QD at fixed $y = 0$ nm and $z = 6$ nm, with x varying from -3.71 to 3.71 nm. The second line is along the z-axis, i.e., at fixed $y = 0$ nm and $x = 0$ nm, with z varying from 2 to 6 nm. The third line is along a specific vertical line where x and y are fixed at 2.15 and 0 nm, with z varying from 2 to 6 nm. All these lines are within the QD so that we can systematically study the features of cubic QD band edges in a half-space.

The strain components and band edge values along the first dashed-dotted line are shown in Figs. 2(a)–2(d) for a cubic QD in GaAs (001) and GaAs (111) substrates. As shown in Figs. 2(a) and 2(c), the biaxial strain γ_B is always positive within the QD domain thus inducing a higher energy level in LH band than in HH band, which is consistent with previous work.[32,36,39] The strain components R_γ and S_γ [expressed by Figs. 2(c) and 2(d)], which represent the contributions from the shear strain and the normal strain difference

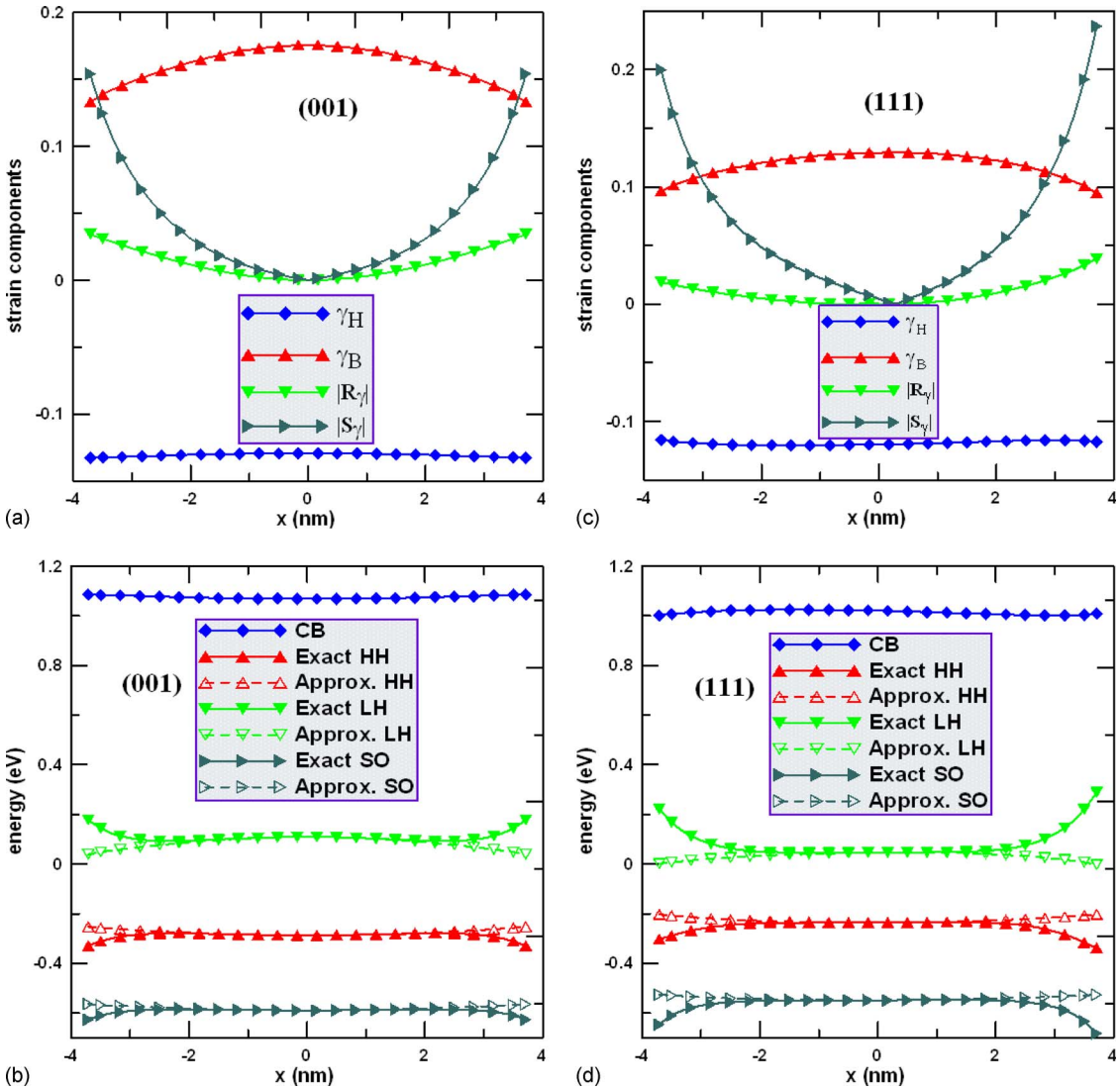

FIG. 2. (Color online) Strain components [(a) and (c)] and band edges [(b) and (d)] in a cubic InAs/GaAs QD along the bottom center line of the QD [(a) and (b)] in (001) substrate and [(c) and (d)] in (111) substrate.

between γ_{xx} and γ_{yy}, clearly indicate that their magnitude increases from the center to the lateral boundary of the QD. Consequently, one would expect that the band edge based on the exact and approximate methods could be different, particularly near the lateral boundary area of the QD. It is also apparent from Figs. 2(b) and 2(d) that the band edge difference between the two methods is larger in the InAs QD embedded in GaAs (111) than that in GaAs (001).

Along the second dashed-dotted line, the shear strain and normal strain difference between γ_{xx} and γ_{yy} are close to zero due to the symmetry of the geometry about the z-axis [R_γ and S_γ shown in Figs. 3(a) and 3(c)]. Therefore, the band edges based on the two methods are nearly identical, even near the boundary of the QD [Figs. 3(b) and 3(d)]. Along the third line, which is an off-center vertical line, R_γ and S_γ are not zero, particularly near the boundary of the QD as in Figs. 4(a) and 4(c). Therefore, some differences in the band edges based on the two methods are observed near the boundary, as shown in Figs. 4(b) and 4(d). Again the difference is larger in GaAs (111) than in GaAs (001).

B. Local band edges in a pyramidal InAs QD embedded in (001) and (111) GaAs half-space substrates

The numerical results for the strain components and local band edges in pyramidal InAs QD embedded in GaAs (001) and GaAs (111) are shown in Figs. 5–7. Figure 5 shows the result along the first dashed-dotted line, i.e., the center line on the bottom of the QD (for $y=0$ nm and $z=6$ nm, with x varying from -7.464 to 7.464 nm). It is obvious that the results are symmetric (on the positive and negative x sides) for the QD in GaAs (001) but is slightly asymmetric in GaAs (111), particularly for the shear strain component [Fig. 5(c)]. Similar to the cubic QD, we observe apparent differences between the approximate and exact methods near the lateral boundary of the QD.

Figure 6 shows the strain components and local band edges along the second dashed-dotted line, i.e., for $x=y=0$ nm with z varying from 2 to 6 nm, within the InAs QD based on both methods. It is clear from Figs. 6(a) and 6(c) that the strain distribution in a pyramidal QD is quite differ-

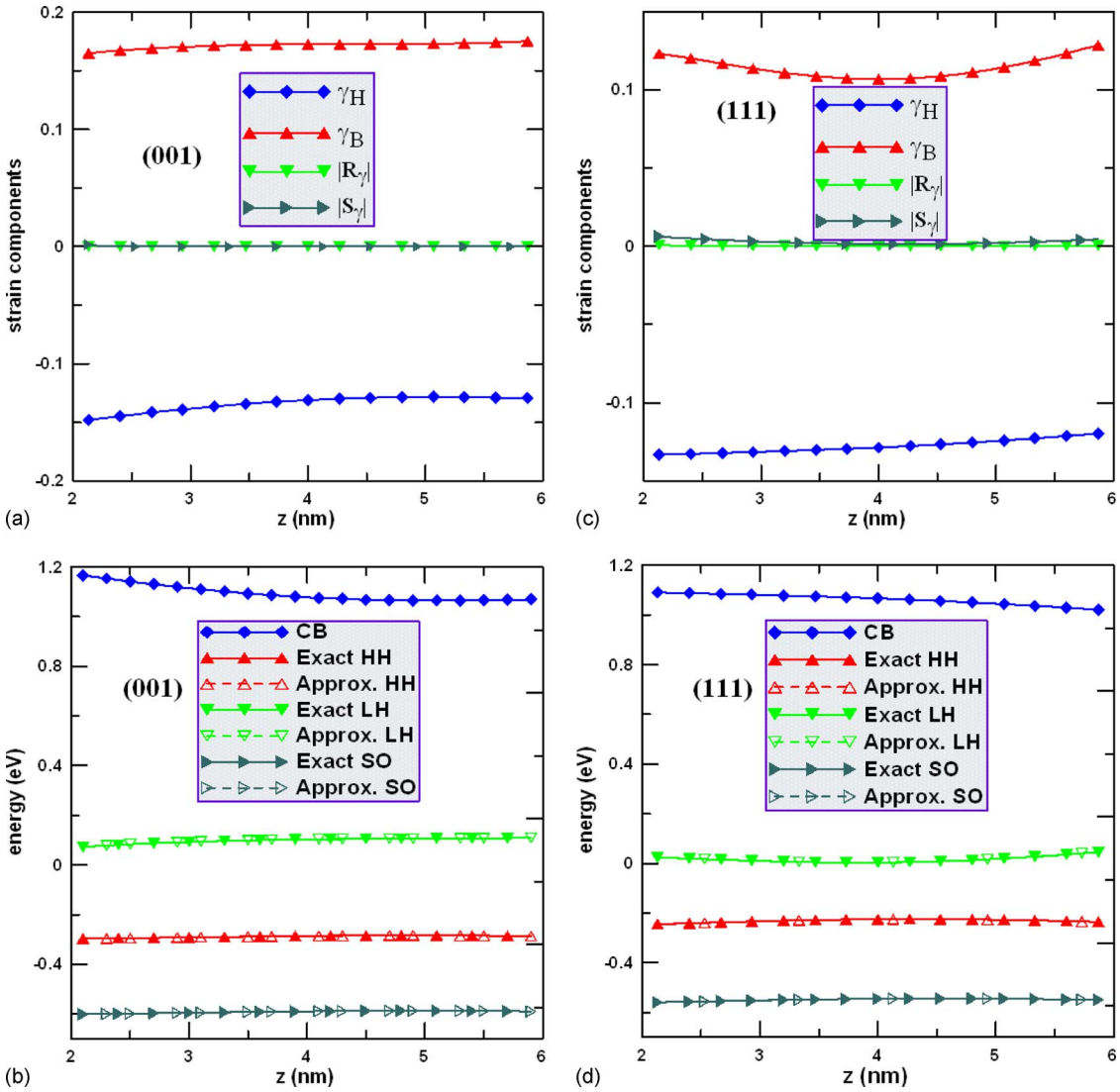

FIG. 3. (Color online) Strain components [(a) and (c)] and band edges [(b) and (d)] in a cubic InAs/GaAs QD along the z-axis of the QD [(a) and (b)] in (001) substrate and [(c) and (d)] in (111) substrate.

ent than that in a cubic QD along this line. For instance, the γ_H has a relatively large change, which induces a large drop in the CB curve near the apex of the pyramid. Furthermore, the energy level of the LH is always higher than that of the HH because of the positive value of γ_B as in cubic QD [Figs. 3(b) and 3(d)]. Finally, Fig. 7 shows the band edge within the pyramidal QD along the third dashed-dotted line, i.e., along the special vertical line at $x=4.33$ nm and $y=0$ nm with z varying from 4.32 to 6 nm. Compared to the other two lines, the studied points are closer to the QD boundary, and thus an apparent difference in the band edge between the approximate and exact methods exists along the entire line, as shown in Figs. 7(b) and 7(d). As in the cubic QD case, the band edge discrepancy in the QD embedded in GaAs (111) is larger than that embedded in GaAs (001).

In summary, there are some interesting features in the QD-induced strain and band edge distributions within the InAs QD embedded in the GaAs (001) and GaAs (111) half-space substrates: First, the γ_H shifts both the CB and VB edges, and both the γ_B and Δ contribute to the splitting between HH and LH while the Δ only introduces the splitting between LH and SO band edges. Second, the band edge of LH is always higher than that of HH because of the positive γ_B. Third, in some cases, large differences in band edges based on the exact and approximate methods may exist in the QD domain, as is further discussed in Sec. III C.

C. Band edge error based on the approximate method

The approximate and exact methods were compared for band edge values at specific locations as depicted in Fig. 1. Among the three lines—one parallel and two perpendicular to the surface of the substrate—the difference between the two calculation methods is the largest for points in the line parallel to the surface. The difference between the two methods is always large near the boundary of the QD. Also, we can see clearly, from Fig. 2 to Fig. 7, that the band edge difference in QDs embedded in the (111)-oriented GaAs substrate is larger than that in QDs embedded in the (001)-oriented substrate.

Here we further study the error in the strain-induced local band edge based on the approximate method where the

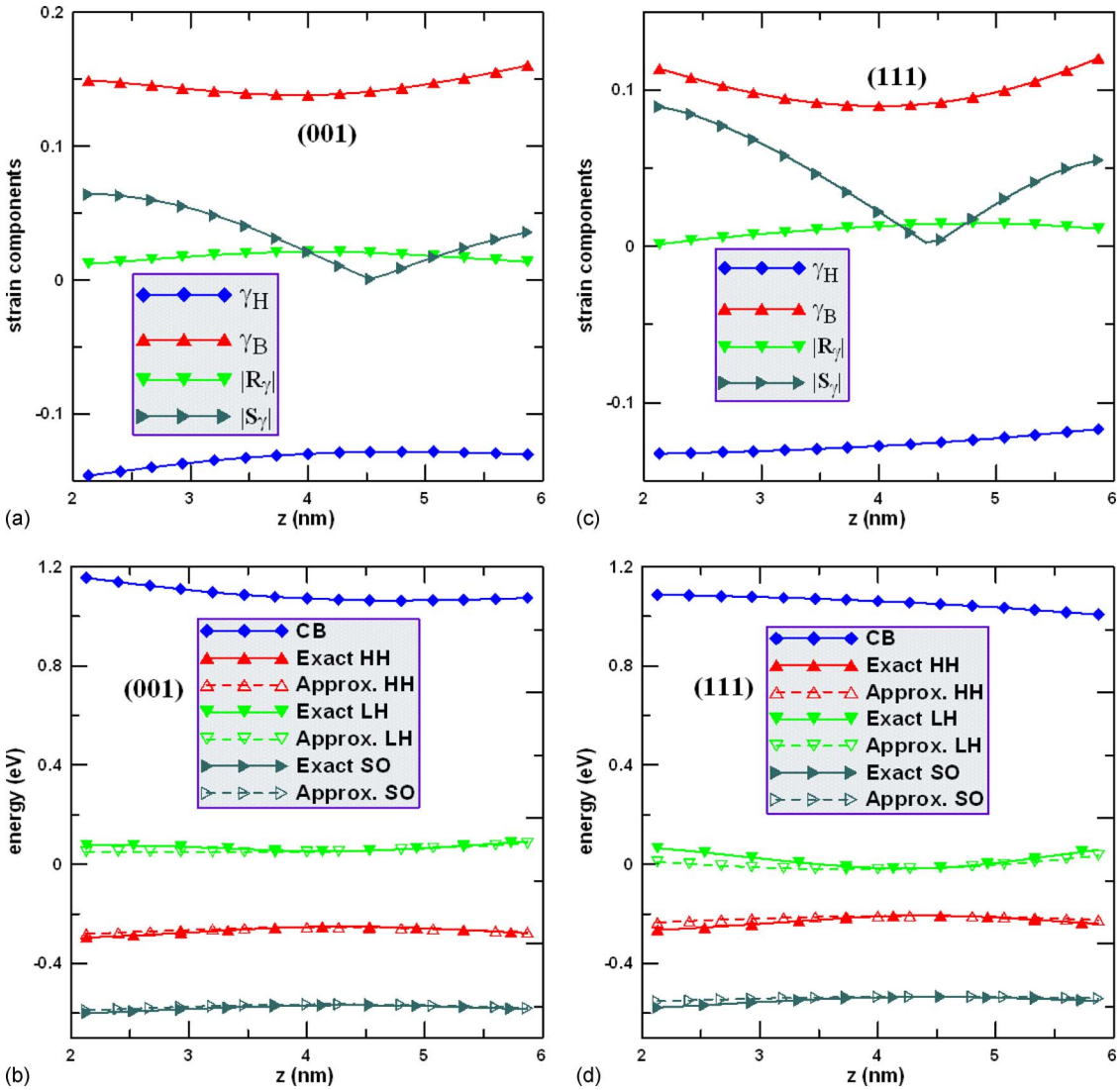

FIG. 4. (Color online) Strain components [(a) and (c)] and band edges [(b) and (d)] in a cubic InAs/GaAs QD along the specified vertical line of the QD [(a) and (b)] in (001) substrate and [(c) and (d)] in (111) substrate.

shear strain and the normal strain difference between γ_{xx} and γ_{yy} are neglected. We define the relative error as

$$\text{error}(\%) = \frac{|E_i - \text{eig}(H)|}{|\text{eig}(H)|} \times 100\%, \tag{6}$$

where E_i refers to the energies calculated from Eqs. (4a)–(4c) using the approximate method, and eig(H) refers to the eigenvalues of Hamiltonian matrix (2) using the exact method. The relative errors are shown in Figs. 8(a) and 8(b) for points along the bottom center line and along the z-axis, respectively, for cubic InAs QD embedded in GaAs half-space substrates with (001) and (111) orientations. It is observed that along the z-axis, the relative error is very small (the biggest error is around 1%) [Fig. 8(b)]; while along the bottom center line of the QD, the relative error can be as large as 100% [Fig. 8(a) near the lateral boundary of the QD]. We also note that the error curves for a QD in the GaAs (111) substrate are asymmetric because of the asymmetric strain and energy distribution [as shown in Figs. 2(c) and 2(d)]. Therefore, along the bottom center line, one has to use the exact eigenvalue solution method to predict the strain field and its induced local band edges.

D. Band edges at different depths

In most previous research on band edge calculation, the QD was assumed to be in an infinite substrate,[31,32,36,37] which means the QD is surrounded by a thick substrate material without any influence from the external boundary or surface. However, QDs are more commonly found located near the interface or covered by a cap layer due to either fabrication procedures or, in some cases, by design to achieve novel device properties.[40–43] In such applications, the effect of the free surface on band edges can be significant. Actually, Nishi *et al.*[41] showed that the thick cap layer can produce a remarkable reduction in the photoluminescence (PL) linewidth; Hugues *et al.*[44] observed that a 5 nm $Ga_{0.85}In_{0.15}As$ cap layer over the InAs QDs led to highly efficient emission of longer

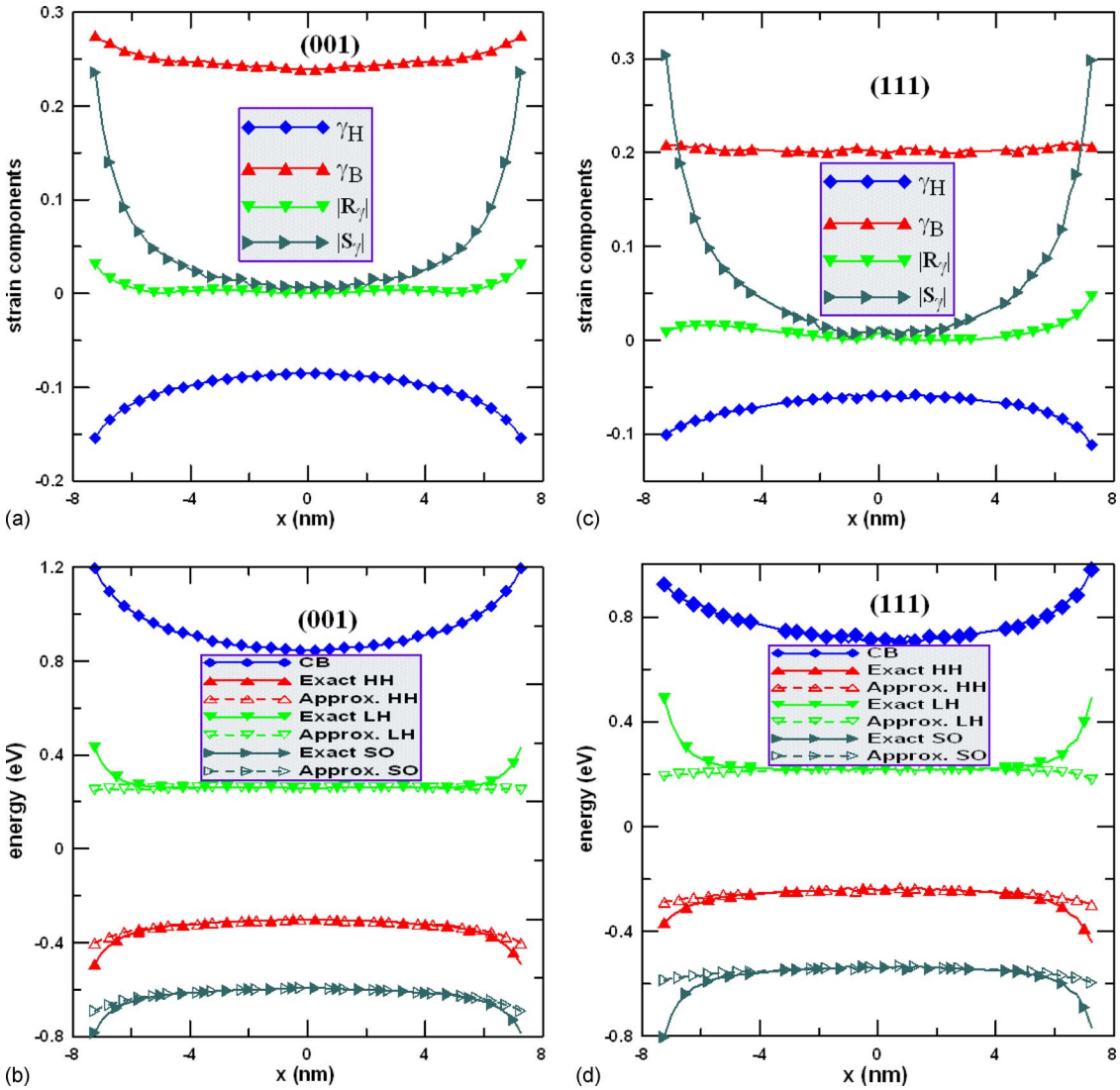

FIG. 5. (Color online) Strain components [(a) and (c)] and band edges [(b) and (d)] in a pyramidal InAs/GaAs QD along the bottom center line of the QD [(a) and (b)] in (001) substrate and [(c) and (d)] in (111) substrate.

wavelength light with the latter being further attributed to the corresponding bandgap energy.

To demonstrate the band edge differences in QDs located at different depths d in half-space substrates, we take the InAs cubic QD [Fig. 1(a)] as the example and use the exact method to carry out the numerical calculation. Shown in Figs. 9 and 10 are the HH, LH, and SO band edge variations along the bottom center line and along the z-axis for different embedding depths of the QD. In Fig. 10, the values -2, 0, and 2 on the z-axis correspond, respectively, to the top, middle height, and bottom positions of the QD [refer to Fig. 1(a) since the height of the QD is 4 nm]. It is clear that when the buried QD is further beneath the free surface, from $d=4$ nm to $d=24$ nm (distance d between the surface and middle height of cubic QD), the band edge curves gradually converge to the infinite-space solution with a decreasing trend. That is, the energy band edge variation becomes less and less as the QD moves away from the surface. This reasonable trend also indicates that when the depth of the QD reaches a critical value (around 14 nm in this example), the substrate is effectively infinite.

E. Comparison with experimental results

We finally compare the energy bandgap from our calculations (both exact and approximate $\mathbf{k}\cdot\mathbf{p}$ models) to previous experimental results[41,44] in order to investigate the effect of the QD depth from the surface and to validate our analytical solutions. In our calculation, the InAs QDs are assumed to be in the $In_xGa_{1-x}As$ substrate with different depths (or different cap layer thicknesses). Both PL measured and calculated bandgap energies are shown in Fig. 11. While we used the same QD size as those in Ref. 41, we chose the InAs QD with a large aspect ratio (base=20 nm; height=5 nm) in order to compare the experimental results in Ref. 44 since no specific size information was available. Furthermore, a large aspect ratio is the general case for capped QDs,[40–42,45] and it is also a dominant factor for band edge energy.[31] We remark that since the PL measured result represents a volumetric average of the actual bandgap in the QD,[4,46] it should therefore correspond to the accurate bandgap distribution predicted based on the exact $\mathbf{k}\cdot\mathbf{p}$ model.

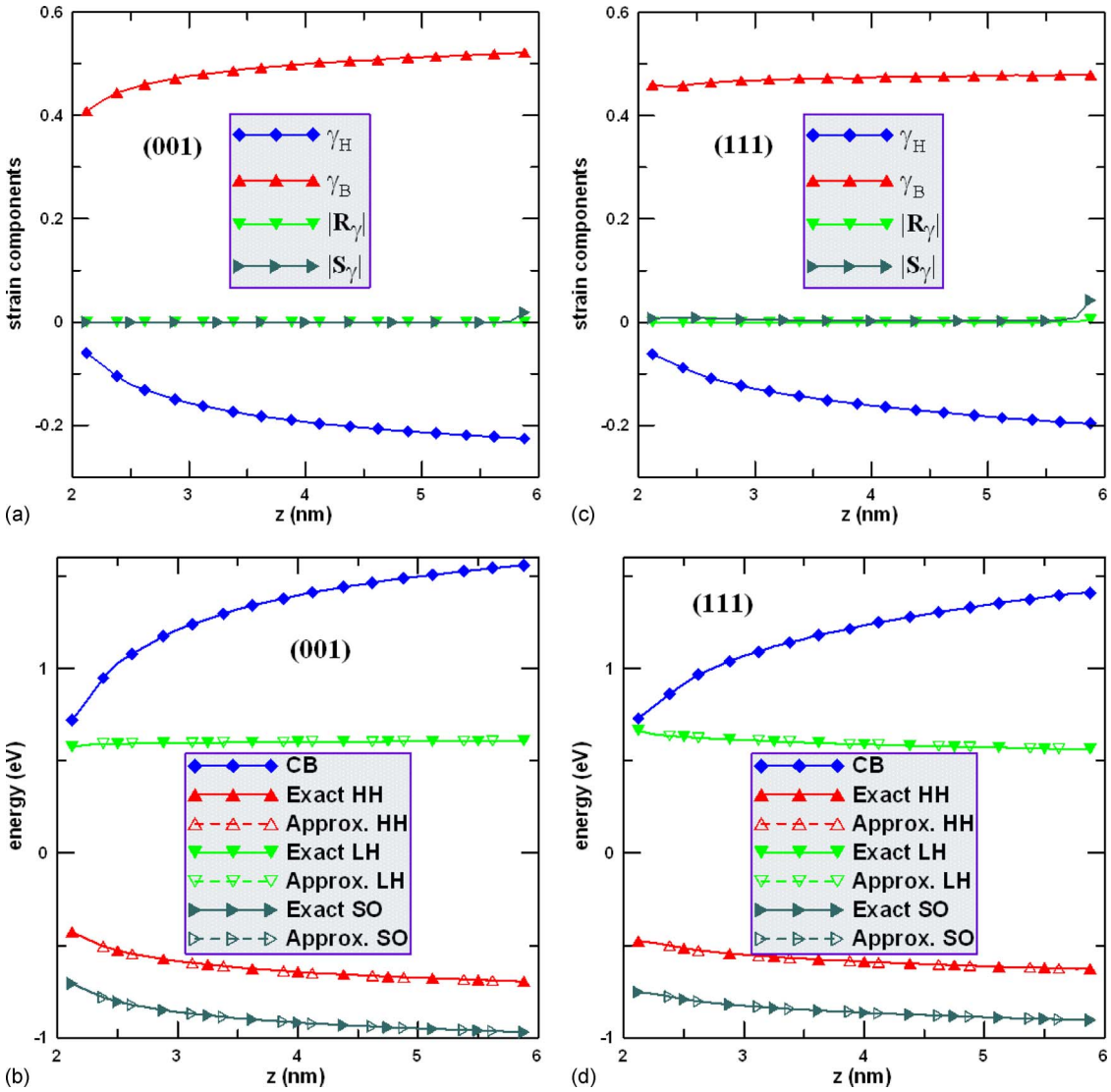

FIG. 6. (Color online) Strain components [(a) and (c)] and band edges [(b) and (d)] in a pyramidal InAs/GaAs QD along the z-axis of the QD [(a) and (b)] in (001) substrate and [(c) and (d)] in (111) substrate.

As shown in Fig. 11, the bandgap energy from our calculation decreases with increasing depth of the QD (or cap layer thickness), which is consistent with the redshift trend observed from experiments. In the limit, the energy level converges to the infinite-space substrate case. These results demonstrate the important effect of the surface on the energy band edge. Furthermore, compared to the experimental results, the bandgap energy based on the simplified approximate $\mathbf{k}\cdot\mathbf{p}$ model showed clearly a larger error than that based on the exact $\mathbf{k}\cdot\mathbf{p}$ model. We point out that the small differences in the energy between the experimental results and exact model could come from the small variation in the QD size and cap layer thickness, which would require precise measurements of these parameters in the future.

IV. CONCLUSIONS

In this article, we have studied the local band edge energies for zincblende InAs QDs in GaAs half-space substrates with full consideration of strains induced by the lattice mismatch and influenced by the free surface. The strain fields are calculated by an accurate CM method based on the Eshelby inclusion model combined with the half-space Green's functions. By virtue of our CM method, a QD with any shape can be approximated by a number of flat triangles so that we can derive an analytical result for the strain fields. This method is particularly efficient when the QD surface is composed of facets.

The strain-induced band edges in cubic and pyramidal InAs QDs (embedded in a GaAs half-space substrate) are then calculated based on two 6×6 $\mathbf{k}\cdot\mathbf{p}$ models (or approaches)—one is inclusive of the detailed strain terms and the other is approximate (the shear strain effect and the difference between the normal strains are neglected). Our numerical results indicate that the approximate model, which has been commonly adopted in literature,[43,44] may lead to significant errors in the band edge energies. This is particularly true for points close to the boundary and/or corner of the QD where a relative error as large as 100% is observed.

We have also calculated the strain-induced band edge in

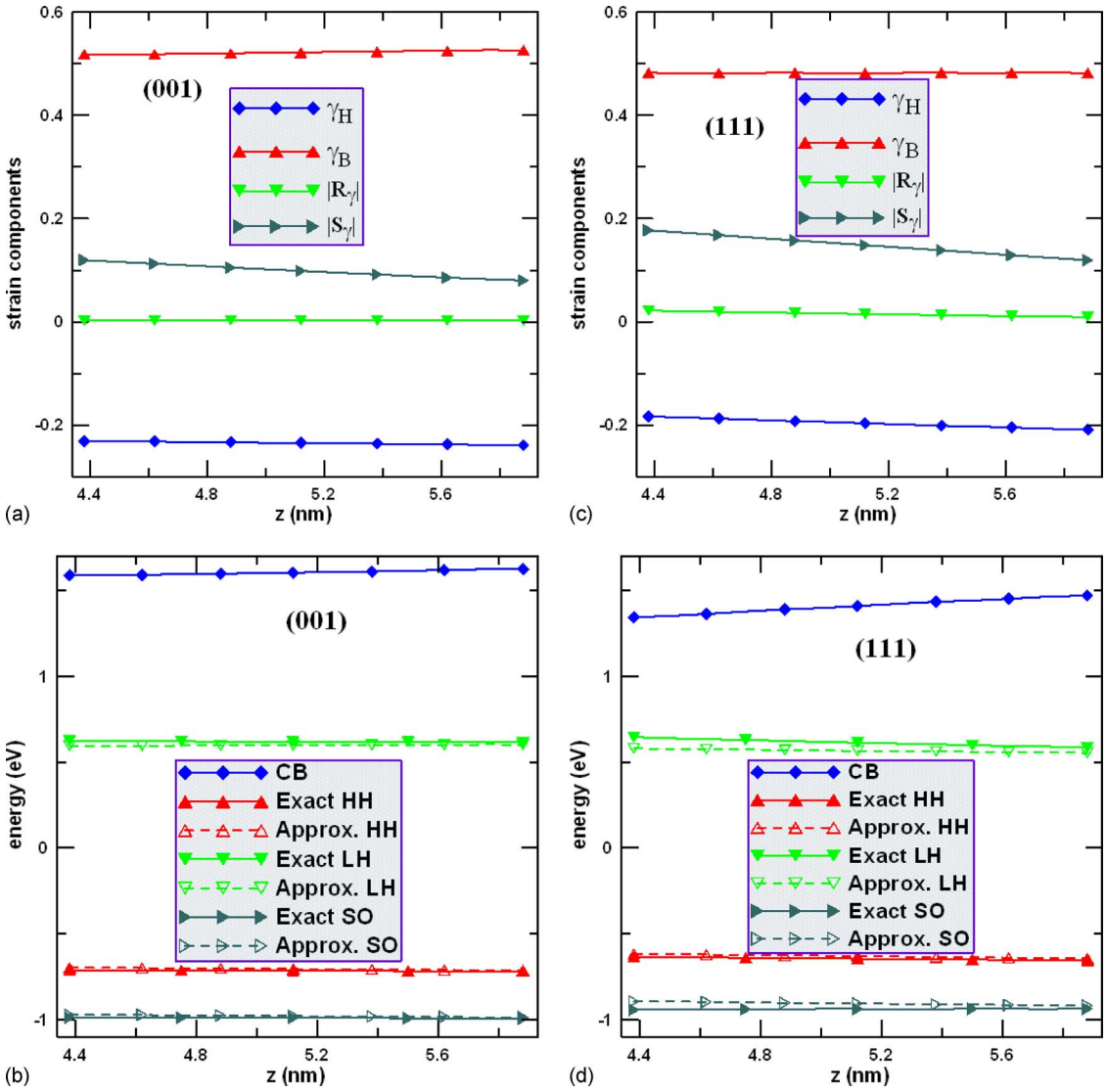

FIG. 7. (Color online) Strain components [(a) and (c)] and band edges [(b) and (d)] in a pyramidal InAs/GaAs QD along the specified vertical line of the QD [(a) and (b)] in (001) substrate and [(c) and (d)] in (111) substrate.

the cubic QD embedded at different depths within the substrate. Our results show that these band edges are sensitive to the depth, indicating the importance of the free surface in band edge predictions. Our numerical results of band edge energies in QDs embedded in half-space substrates are further compared with existing experimental results. Such a comparison demonstrates that the analytical predictions based on the half-space substrate model with the exact $\mathbf{k}\cdot\mathbf{p}$ approach agree well with the experimental results while the approximate $\mathbf{k}\cdot\mathbf{p}$ approach shows an obvious and significant difference.

ACKNOWLEDGMENTS

This work was partially supported by the National Natural Science Foundation of China Grant No. 10772106 (E.P.), by the Defense Threat Reduction Agency Joint Science and Technology Office (DTRA-JSTO) under Grant No. W911NF-06-2-0038 (E.P. and P.W.C.), and by AFOSR Grant No. FA9550-06-1-0317 (Y.Z. and E.P.). The authors would also like to thank the reviewer for his/her helpful comments and suggestions.

APPENDIX: STIFFNESS MATRICES OF GaAs AND InAs, AND BANDGAP PARAMETERS OF InAs

1. Stiffness matrix C_{ij} in (10^9 N/m^2)

The following are values for stiffness matrix C_{ij} (Ref. 27):

$$[C_{\mathrm{GaAs}(001)}] = \begin{bmatrix} 118.8 & 53.8 & 53.8 & 0.0 & 0.0 & 0.0 \\ & 118.8 & 53.8 & 0.0 & 0.0 & 0.0 \\ & & 118.8 & 0.0 & 0.0 & 0.0 \\ & & & 59.4 & 0.0 & 0.0 \\ & & & & 59.4 & 0.0 \\ & & & & & 59.4 \end{bmatrix} \quad \text{(A1)}$$

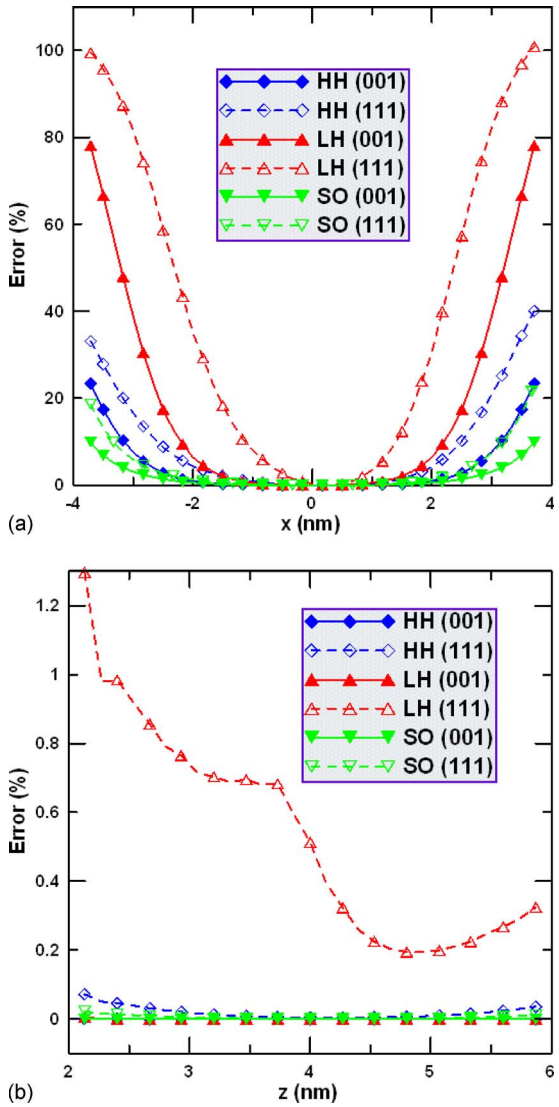

FIG. 8. (Color online) Relative error (%) of the band edge calculations based on the approximate method as compared to the present exact method in an InAs/GaAs cubic QD embedded in GaAs (001) and (111) substrates: results along the bottom center line of the QD in (a) and along the z-axis of the QD in (b).

$$[C_{\mathrm{GaAs(111)}}] = \begin{bmatrix} 145 & 45 & 36 & 0.0 & 12.7 & 0.0 \\ & 145 & 36 & 0.0 & -12.7 & 0.0 \\ & & 154 & 0.0 & 0.0 & 0.0 \\ & & & 41 & 0.0 & -12.7 \\ & & & & 41 & 0.0 \\ & & & & & 50 \end{bmatrix} \quad \text{(A2)}$$

$$[C_{\mathrm{InAs(001)}}] = \begin{bmatrix} 83.29 & 45.26 & 45.26 & 0.0 & 0.0 & 0.0 \\ & 83.29 & 45.26 & 0.0 & 0.0 & 0.0 \\ & & 83.29 & 0.0 & 0.0 & 0.0 \\ & & & 39.59 & 0.0 & 0.0 \\ & & & & 39.59 & 0.0 \\ & & & & & 39.59 \end{bmatrix} \quad \text{(A3)}$$

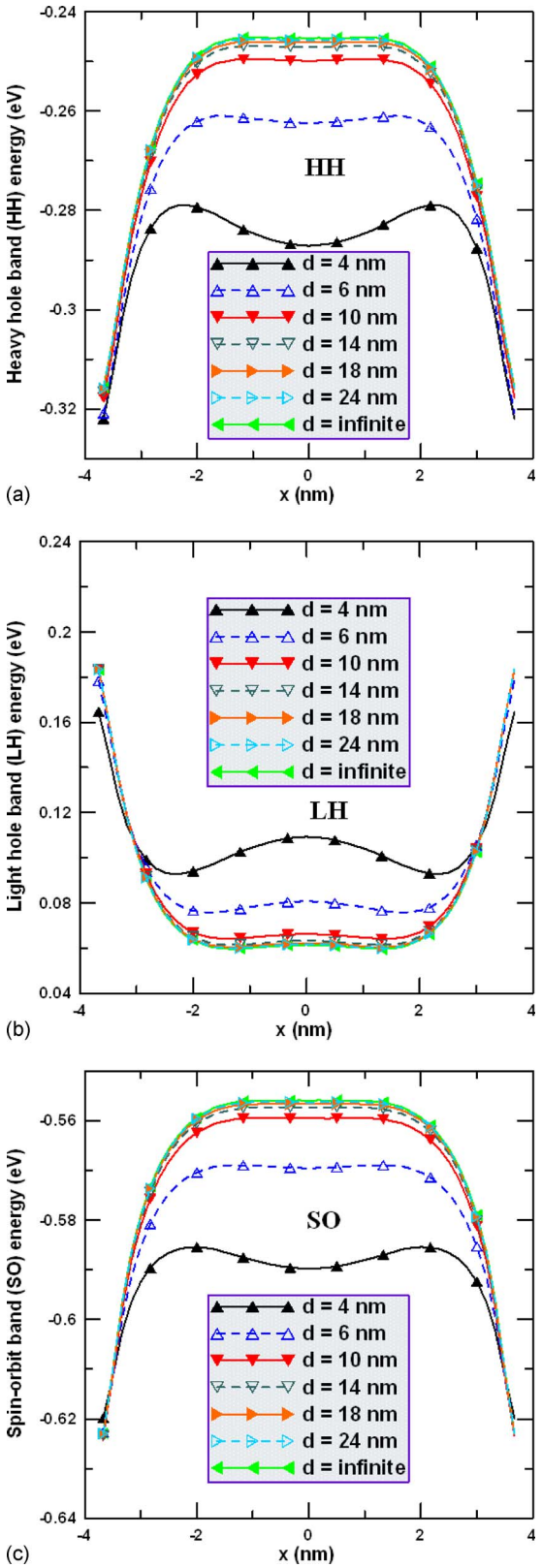

FIG. 9. (Color online) Band edges in a cubic QD embedded at different depths within the GaAs half-space substrate and in the infinite-space substrate along the bottom center line of the QD: (a), (b), and (c) refer to the HH, LH, and SO bands, respectively.

2. Band parameters (in eV) for InAs

The following are band parameters for InAs (Ref. 30):

$E_{g0} = 0.413$,

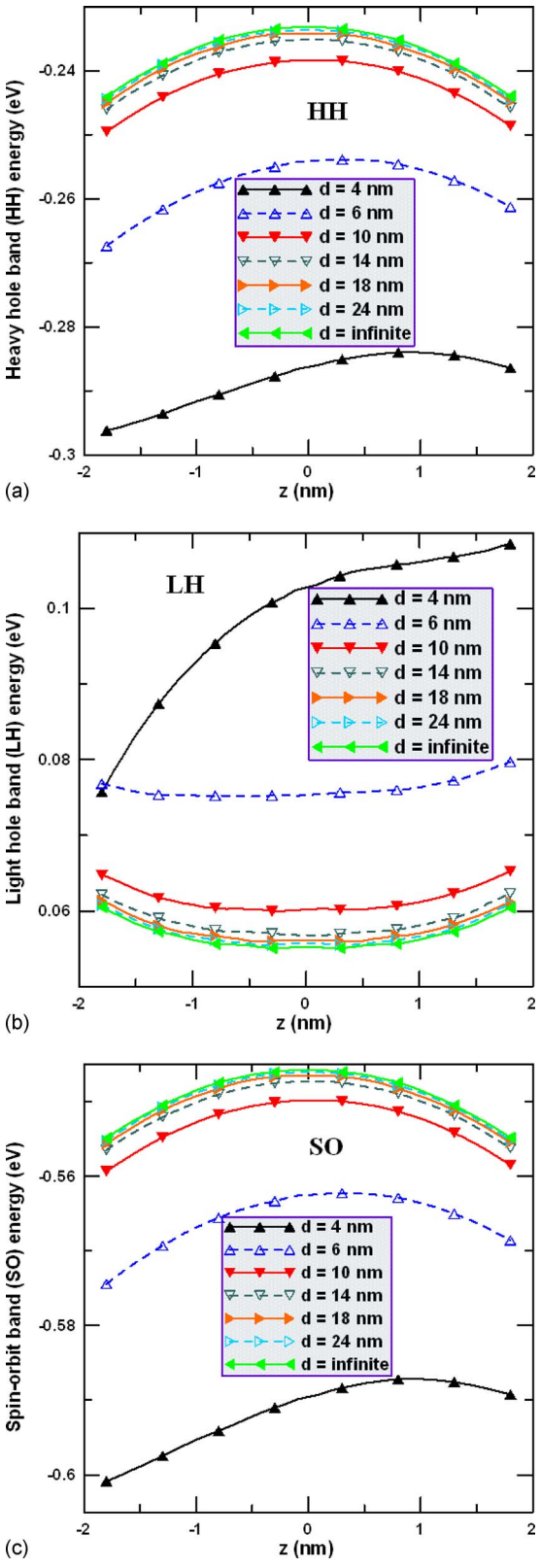

FIG. 10. (Color online) Band edges in a cubic QD embedded at different depths within the GaAs half-space substrate and in the infinite-space substrate along the z-axis of the QD: (a), (b), and (c) refer to the HH, LH, and SO bands, respectively.

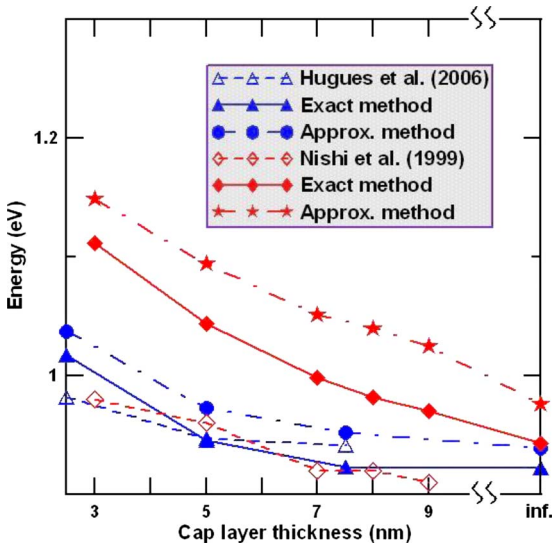

FIG. 11. (Color online) Comparison of bandgap energies between the experimental results and present calculations for InAs QDs within $In_xGa_{1-x}As$ substrates (the $\mathbf{k}\cdot\mathbf{p}$ calculations are based on both the exact and approximate methods).

$$\Delta_{SO} = 0.38,$$

$$a_c = -5.08,$$

$$a_v = 1.00,$$

$$b = -1.80,$$

$$d = -3.60.$$

[1]D. Bimberg, M. Grundmann, and N. N. Ledentsov, *Quantum Dot Heterostructures* (Wiley, New York, 1999).
[2]J. Piprek, *Semiconductor Optoelectronic Devices* (Academic, New York, 2003).
[3]P. Y. Yu and M. Cardona, *Fundamentals of Semiconductors* (Springer, New York, 2005).
[4]H. Zhu, S. Feng, D. Jiang, Y. Deng, and H. Wang, Jpn. J. Appl. Phys., Part 1 **38**, 6264 (1999).
[5]K. Kamath, H. Jiang, D. Klotzkin, J. Phillips, T. Sosnowski, T. Norris, J. Singh, and P. Bhattacharya, IEEE International Symposium on Compound Semiconductors, 1997 (unpublished), p. 525.
[6]A. D. Andreev and E. P. O'Reilly, Phys. Rev. B **62**, 15851 (2000).
[7]V. Ranjan, G. Allan, C. Priester, and C. Delerue, Phys. Rev. B **68**, 115305 (2003).
[8]M. Grundmann, O. Stier, and D. Bimberg, Phys. Rev. B **52**, 11969 (1995).
[9]M. Califano and P. Harrison, J. Appl. Phys. **91**, 389 (2002).
[10]C. Pryor, J. Kim, L. W. Wang, A. J. Williamson, and A. Zunger, J. Appl. Phys. **83**, 2548 (1998).
[11]H. T. Johnson, L. B. Freund, C. D. Akyuz, and A. Zaslavsky, J. Appl. Phys. **84**, 3714 (1998).
[12]A. D. Andreev, J. R. Downes, D. A. Faux, and E. P. O'Reilly, J. Appl. Phys. **86**, 297 (1999).
[13]H. T. Johnson and L. B. Freund, Int. J. Solids Struct. **38**, 1045 (2001).
[14]A. J. Williamson, L. W. Wang, and A. Zunger, Phys. Rev. B **62**, 12963 (2000).
[15]M. Tadic, F. M. Peeters, K. L. Janssens, M. Korkusinski, and P. Hawrylak, J. Appl. Phys. **92**, 5819 (2002).
[16]L. C. Lew Yan Voon and L. R. Ram-Mohan, Phys. Rev. B **47**, 15500 (1993).
[17]E. Lidorikis, M. M. Sigalas, E. N. Economou, and C. M. Soukoulis, Phys. Rev. Lett. **81**, 1405 (1998).
[18]W. A. Harrison, Phys. Rev. B **77**, 245103 (2008).
[19]A. Valavanis, Z. Ikonic, and R. W. Kelsall, Phys. Rev. B **75**, 205332

(2007).
[20]P. Piquini, A. Zunger, and R. Magri, Phys. Rev. B **77**, 115314 (2008).
[21]O. Stier, M. Grundmann, and D. Bimberg, Phys. Rev. B **59**, 5688 (1999).
[22]E. Pan, Y. Zhang, P. W. Chung, and M. Denda, Comput. Model. Eng. Sci. **841**, 1 (2008).
[23]T. C. T. Ting, *Anisotropic Elasticity Theory and Applications* (Oxford Science, New York, 1996).
[24]E. Pan, Proc. R. Soc. London, Ser. A **458**, 181 (2002).
[25]C. Y. Wang, M. Denda, and E. Pan, Int. J. Solids Struct. **43**, 7593 (2006).
[26]E. Pan and B. Yang, J. Appl. Phys. **90**, 6190 (2001).
[27]E. Pan, J. Appl. Phys. **91**, 6379 (2002).
[28]B. Yang and E. Pan, J. Appl. Phys. **92**, 3084 (2002); E. Pan, F. Han, and J. D. Albrecht, *ibid.* **98**, 013534 (2005).
[29]S. W. Ellaway and D. A. Faux, J. Appl. Phys. **92**, 3027 (2002).
[30]I. Vurgaftman, J. R. Meyer, and L. R. Ram-Mohan, J. Appl. Phys. **89**, 5815 (2001).
[31]S. I. Rybchenko, G. Yeap, R. Gupta, I. E. Itskevich, and S. K. Haywood, J. Appl. Phys. **102**, 013706 (2007).
[32]A. Schliwa, M. Winkelnkemper, and D. Bimberg, Phys. Rev. B **76**, 205324 (2007).
[33]C. Y. Chao and S. L. Chuang, Phys. Rev. B **46**, 4110 (1992).
[34]J. M. Luttinger and W. Kohn, Phys. Rev. **97**, 869 (1955).
[35]G. L. Bir and G. E. Pikus, *Symmetry and Strain-Induced Effects in Semiconductors* (Wiley, New York, 1974).
[36]C. Pryor, Phys. Rev. B **57**, 7190 (1998).
[37]C. Pryor, M.-E. Pistol, and L. Samuelson, Phys. Rev. B **56**, 10404 (1997).
[38]E. Pan, J. Appl. Phys. **91**, 3785 (2002).
[39]M. A. Cusack, P. R. Briddon, and M. Jaros, Phys. Rev. B **54**, R2300 (1996).
[40]K. Mukai and M. Sugawara, Appl. Phys. Lett. **74**, 3963 (1999).
[41]K. Nishi, H. Saito, S. Sugou, and J. S. Lee, Appl. Phys. Lett. **74**, 1111 (1999).
[42]Z. Gong, Z. D. Fang, Z. H. Miao, Z. C. Niu, and S. L. Feng, J. Cryst. Growth **274**, 78 (2005).
[43]M. Richter, B. Damilano, J. Y. Duboz, J. Massies, and A. D. Wieck, Appl. Phys. Lett. **88**, 231902 (2006).
[44]M. Hugues, M. Richter, B. Damilano, J. M. Chauveau, J. Y. Duboz, J. Massies, and A. D. Wieck, Phys. Status Solidi C **3**, 3979 (2006).
[45]J. Tatebayashi, M. Nishioka, and Y. Arakawa, Appl. Phys. Lett. **78**, 3469 (2001).
[46]Z. L. Miao, Y. W. Zhang, S. J. Chua, Y. H. Chye, P. Chen, and S. Tripathy, Appl. Phys. Lett. **86**, 031914 (2005).